energies

Article

Assessing the Geothermal Potential of Selected Depleted Oil and Gas Reservoirs Based on Geological Modeling and Machine Learning Tools

Tomasz Topór [1,*], Małgorzata Słota-Valim [1] and Rafał Kudrewicz [2]

[1] Oil and Gas Institute—National Research Institute, 25 A Lubicz Str., 31-503 Cracow, Poland; slota-valim@inig.pl
[2] PKN Orlen-PGNiG Exploration & Production Division, Kasprzaka 25a, 01-224 Warszawa, Poland; rafal.kudrewicz@pgnig.pl
* Correspondence: topor@inig.pl; Tel.: +48-126177686

Abstract: The study evaluates the geothermal energy potential of two depleted oil and gas reservoirs representing two different lithostratigraphic formations—the carbonate formation of the Visean age from the basement of the Carpathian Flysch and the Rotliegend sandstone formation from the Eastern part of the Foresudetic Monocline, Poland. Advanced modeling techniques were employed to analyze the studied formations' heat, storage, and transport properties. The obtained results were then used to calculate the heat in place (HIP) and evaluate the recoverable heat (Hrec) for both water and CO_2 as working fluids, considering a geothermal system lifetime of 50 years. The petrophysical parameters and Hrec were subsequently utilized in the generalized c-means (GFCM) clustering analysis, which helped to identify plays with the greatest geothermal potential within the studied formations. The central block emerged as the most promising area for the studied carbonate formation with Hrec values of ~1.12 and 0.26 MW when H_2O and CO_2 were used as working fluids, respectively. The central block has three wells that can be easily adapted for geothermal production. The area, however, may require permeability enhancement techniques to increase reservoir permeability. Two prospective zones were determined for the analyzed Rotliegend sandstone formation: one in the NW region and the other in the SE region. In the NW region, the estimated Hrec was 23.16 MW and 4.36 MW, while in the SE region, it was 19.76 MW and 3.51 MW, using H_2O and CO_2 as working fluids, respectively. Both areas have high porosity and permeability, providing good storage and transport properties for the working fluid, and abundant wells that can be configured for multiple injection-production systems. When comparing the efficiency of geothermal systems, the water-driven system in the Visean carbonate formation turned out to be over four times more efficient than the CO_2-driven one. Furthermore, in the case of the Rotliegend sandstone formation, it was possible to access over five times more heat using water-driven system.

Keywords: machine learning; GFCM clustering; geological modeling; geothermal resource exploration

check for updates

Citation: Topór, T.; Słota-Valim, M.; Kudrewicz, R. Assessing the Geothermal Potential of Selected Depleted Oil and Gas Reservoirs Based on Geological Modeling and Machine Learning Tools. *Energies* **2023**, *16*, 5211. https://doi.org/10.3390/en16135211

Academic Editors: Jadwiga A. Jarzyna, Bogdan Mihai Niculescu and Edyta Puskarczyk

Received: 5 June 2023
Revised: 29 June 2023
Accepted: 2 July 2023
Published: 6 July 2023

1. Introduction

Geothermal energy is foreseen to play a significant role in the future energy mix as a promising resource that can be sustainably utilized. In the context of climate change and the recent geopolitical situation in Europe, geothermal energy is becoming a critical element for energy security strategies and climate policy goals [1]. Geothermal energy is also an excellent alternative to the combustion of fossil fuels and some weather-dependent renewable resources. It has a long lifetime that can be extended up to 100 years and low greenhouse gas (GHG) emissions during its lifecycle [2,3].

Among many types of geothermal resources, the low-enthalpy (<150 °C) geothermal heat locked in hot sedimentary aquifers creates an attractive target for geothermal system development [4,5]. A significant advantage of low-enthalpy geothermal systems is their widespread availability, which offers worldwide potential for energy production [5–7].

Depleted oil and gas reservoirs take a special place in low-enthalpy systems. The experience gained from the reservoir evaluation and production phases, along with the availability of existing infrastructure, causes them to be easily adapted as geothermal resources [8]. Most depleted oil and gas reservoirs belong to enhanced or engineered geothermal systems (EGS) that require technology to increase reservoir productivity. The enhancement is accomplished by increasing permeability and/or introducing extra fluid to the reservoir [7]. The EGS resources are most often utilized through a system of geothermal doublets comprising two wells—one for cold water injection and another for hot water production. The accurate doublet configuration is crucial for predicting lifetime and energy production [9,10]. It thus directly impacts the technical and economic feasibility of geothermal projects and is essential for the successful design of such systems [11].

In the case where heat transfer is realized with CO_2 as a working fluid [12], the geothermal system could be coupled with carbon capture and storage (CCS) [13,14]. This operation can potentially limit the operational cost of such a combined system and contribute to overall CO_2 emission reduction [15,16].

Projects that explore the feasibility and potential of geothermal energy from depleted reservoirs are conducted in many countries [8,16–20]. In Poland, several studies have been conducted on the characterization of geological conditions of geothermal resource occurrences [21,22], analyses of permeability and porosity of sedimentary rocks in terms of unconventional geothermal resource explorations [23], and evaluating multi-criteria for supporting the selection of locations and technologies used in CO_2-EGS systems [24]. Additionally, several rich source monographs contain information on the occurrence and exploitation potential of geothermal waters and energy in Poland [25–29].

Selecting the best doublet configuration should precede a detailed analysis of crucial reservoir parameters important for successful geothermal energy production. The process involves integrating a significant amount of data, using complex modeling techniques, and managing many uncertainties. Recent advances in machine learning (ML) methods have helped overcome some challenges connected to geothermal exploration. Okoroafor et al. [30] reviewed the application of ML methods in subsurface geothermal energy exploration for the last two decades. These authors indicate seven research areas for which ML tools have been successfully applied: exploration, seismicity, drilling, petrophysics, reservoir characterization, reservoir engineering, and production/injection engineering.

One of the areas in which ML plays a significant role is the identification of favorable geothermal objectives [31]. So far, most of the published studies deal with the evaluation of the geothermal potential via integrating multiple data sources such as geological, geochemical, geophysical, and remote sensing data for the effective mapping of promising areas for further detailed geothermal exploration work. These, however, are regional studies devoted to virgin areas where no or limited information from wells exists. Yusuf et al. [32] provide an overview of such studies. The authors briefly describe 28 studies conducted in countries and regions: USA, Egypt, Nigeria, Turkey, Iran, and New Zealand. Among them, only one integrates multi-criteria evaluation with ML tools such as Fuzzy prediction modeling [33]. Another study that uses ML tools (particularly k-means clustering) in geothermal resource exploration was published by Mudunuru et al. [34]. The ML techniques have been focused mainly on integrating surface geochemistry data for reservoir temperature classification [35], selecting hidden signatures representative of the geothermal resource, and choosing potential geothermal sites [36].

The presented study integrates a comprehensive evaluation of reservoir parameters and the ML classification method to identify areas with the highest geothermal potential in two depleted oil and gas reservoirs in Poland. The studied reservoirs belong to the Visean age's carbonate formation from the Carpathian Flysch basement and the Rotliegend sandstone formation from the Eastern part of the Foresudetic Monocline.

The geothermal reservoir characteristics combine the assessment of the reservoir rock's storage, transport, and thermal properties with calculated heat in place (HIP) and estimated recoverable heat (Hrec) for water and CO_2 systems for a 50-year lifetime. The selected parameters obtained from reservoir modeling (porosity, permeability, and Hrec) are then used in generalized c-means (GFCM) clustering to identify the areas with the highest geothermal potential, expressed in high Hrec, enhanced permeability, and the presence of well infrastructure. Finally, the Hrec for water and CO_2 is compared for the favorable exploration plays in the studied depleted oil and gas reservoirs, and the advantages of selected reservoir types and fluids are discussed. The approach allows for a more accurate characterization of the geothermal plays, which can help mitigate the uncertainty connected to geothermal energy development.

2. Geological Settings

In the study, two different reservoir rocks from two fields were investigated. The first one was a reservoir formation from the oil field, situated in the basement of the Carpathian Flysch, in the SW of Rzeszów. The oil accumulation is related to the anticlinal structure extending towards SEE-NWW. It occurs in a complex of carbonate rocks, represented by limestones and dolomitic limestones of Visean (lower carboniferous) age. The thickness of the carbonate reservoir varies from 45 to 206 m. The reservoir rock properties are moderate, with effective porosity (including fractures) ranging from 2.7 to 4.3% and a 25.8 to 27.1 mD permeability.

The second analyzed reservoir was the Rotliegend sandstone formation from the gas field, located in the Western part of the Foresudetic Monocline. These sandstones, belonging to the Saxonian sub-group of the Rotliegend, are developed in the eolic depositional system and are characterized by a low clay content. The thickness of the sandstone formation varies from 34.26 to 123.85 m, with an average value of 75.37 m. The reservoir rock, with high porosity of approximately 18% in the gas-saturated zone, shows poor differentiation in the vertical section. The results of reservoir characterization revealed that the analyzed Rotliegend sandstones have good reservoir properties in the lower part and poor reservoir quality on the top (unpublished report). The gas accumulates in a structural trap [37] elongated in the NW-SE direction. The culmination of the trap is adjacent to the fault zone, limiting the gas field to the SW. In cross-sections, the analyzed depleted gas reservoir has the shape of a wedge inclined towards the NE.

3. Methods

The methodology adopted in this study comprises two stages. In the first one, key geothermal parameters were derived from a combination of 3D numerical modeling and the estimation method of the HIP, allowing the assessment of the geothermal potential of the reservoir rock. The second stage is derived from the first stage and deploys unsupervised machine learning classification based on pre-selected geothermal parameters to find the best geothermal areas within the studied fields.

3.1. Parametrization of Geothermal Plays

To estimate the energy potential of the geothermal system, it is necessary to know the rock volume and the effective space that would allow for working fluid storage in the reservoir rock. The first can be easily estimated using the structural maps of the reservoir's top and bottom, while the pore space can be determined from effective porosity. Another critical element would be an estimation of the formation's ability to transmit the working fluids—expressed as permeability. As the subject of the study is to investigate the geothermal systems' energy potential, the temperature conditions in the reservoir formation also need to be considered.

The formation thickness of both analyzed reservoir rocks was calculated within the data preparation step. At the same time, the petrophysical properties, such as effective porosity and permeability, were averaged from the developed 3D models of these properties.

The development of spatial distributions of porosity and permeability and other parameters used for the evaluation of the geothermal potential were modeled in Petrel software (Schlumberger). The 3D porosity and permeability models of complex carbonate formations were developed based on 3D seismic and well-log data interpretations from ten wells, which were calibrated with the laboratory measurements of porosity performed on the core material. The 3D parametric models of the Rotliegend sandstone formation were based on well-log data interpretation in ten wells only, as no 3D seismic data were available.

Before calculating their spatial distributions, all modeled parameters were averaged (up-scaled) in intervals corresponding to the vertical resolution of the 3D grid. The interpretations of well data were subjected to geostatistical analysis individually for each modeled parameter, together with the assessment of the anisotropy of reservoir parameters with the use of variogram modeling.

3.1.1. Effective Porosity

The spatial distribution of the effective porosity was modeled based on the results of well-log interpretations calibrated by measurements of the effective porosity of the core samples.

The average value of the porosity in the studied carbonate complex in the entire Visean section, calculated for all wells that drilled the reservoir, is 2.87%. Slightly higher values of effective porosity (3.4%) are observed in the zone with oil accumulation. In the case of the Rotliegend sandstone formation, the measured porosity is much higher, ranging from 1.96 to 28.08%, with an average value of 17.93%. The spatial distribution of the effective porosity in both investigated reservoirs was calculated using the Gaussian random function simulation algorithm, repeating the simulation process ten times.

3.1.2. Absolute Permeability

The absolute permeability 3D model was based on well-log data interpreted by the application of the Zawisza model [38].

The values of absolute permeability within the studied carbonate reservoir varied from 0.04 to 365 mD, with an average value of 36 mD. The permeability in the Rotliegend sandstone formation was 0 to 679 mD, with an average value of 102 mD.

A strong relationship between porosity and permeability was observed during the modeling results analysis. The correlation reflected a method adopted at the well-log data interpretation stage. As a result, the nature of the permeability anisotropy in the spatial model reflects the variability of porosity. This relationship was transferred while calculating the spatial distribution of permeability using the co-kriging option with the spatial porosity model as a parameter controlling the permeability distribution. Like the 3D porosity modeling, the Gaussian random function simulation was used, repeating the calculation process ten times and averaging the resulting distributions to obtain the final 3D model of permeability.

3.1.3. Temperature

The 3D temperature distribution was initially modeled based on the formation temperature logs recorded at particular intervals under perturbed conditions in three wells in the case of the carbonate reservoir and eight wells in the case of the sandstone reservoir. Figure 1 shows the average values obtained for the above-mentioned parameters for the carbonate reservoir and Figure 2 for the sandstone one.

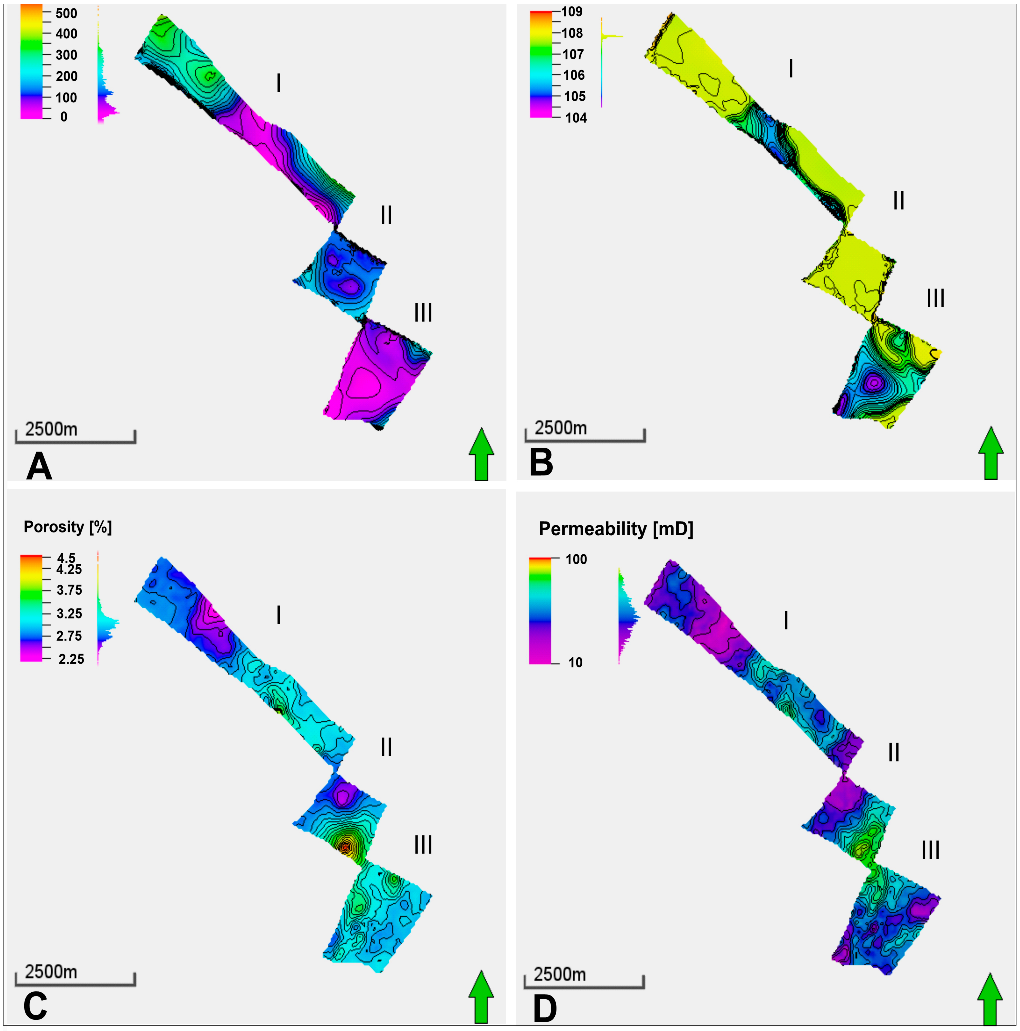

Figure 1. Visualization maps of thickness (**A**), average temperature (**B**), average porosity (**C**), and permeability (**D**) in the carbonate oil reservoir.

3.1.4. Heat in Place

The heat in place methodology was used to estimate the geothermal potential of the analyzed reservoir rocks [39]. This parameter was initially proposed in the 1970s by the United States Geological Survey [40,41] and later modified in more recent studies. It combines rock volume, average reservoir temperature, reference temperature, and the properties characterizing the water-rock system, such as density, porosity, and specific heat capacity of particular system components. In this study, the following formula was used to estimate HIP in the two analyzed reservoirs [42]:

$$\mathrm{HIP} = \mathrm{V} \times (\varphi \times \rho_{\mathrm{F}} \times \mathrm{C_F} + (1 - \varphi) \times \rho_{\mathrm{R}} \times \mathrm{C_R}) \times (\mathrm{T_r} - \mathrm{T_0}) \quad (1)$$

where:
V—rock volume (m^3),
ρ_F and ρ_R—fluid and rock matrix density (kg/m^3), respectively,
C_F, C_R—fluid and rock matrix heat capacity (kJ/(kg °C)),
φ—effective porosity (parts per unit),
T_r and T_0—the temperature at the top of the reservoir, and T_0 is the mean surface temperature (°C), respectively.

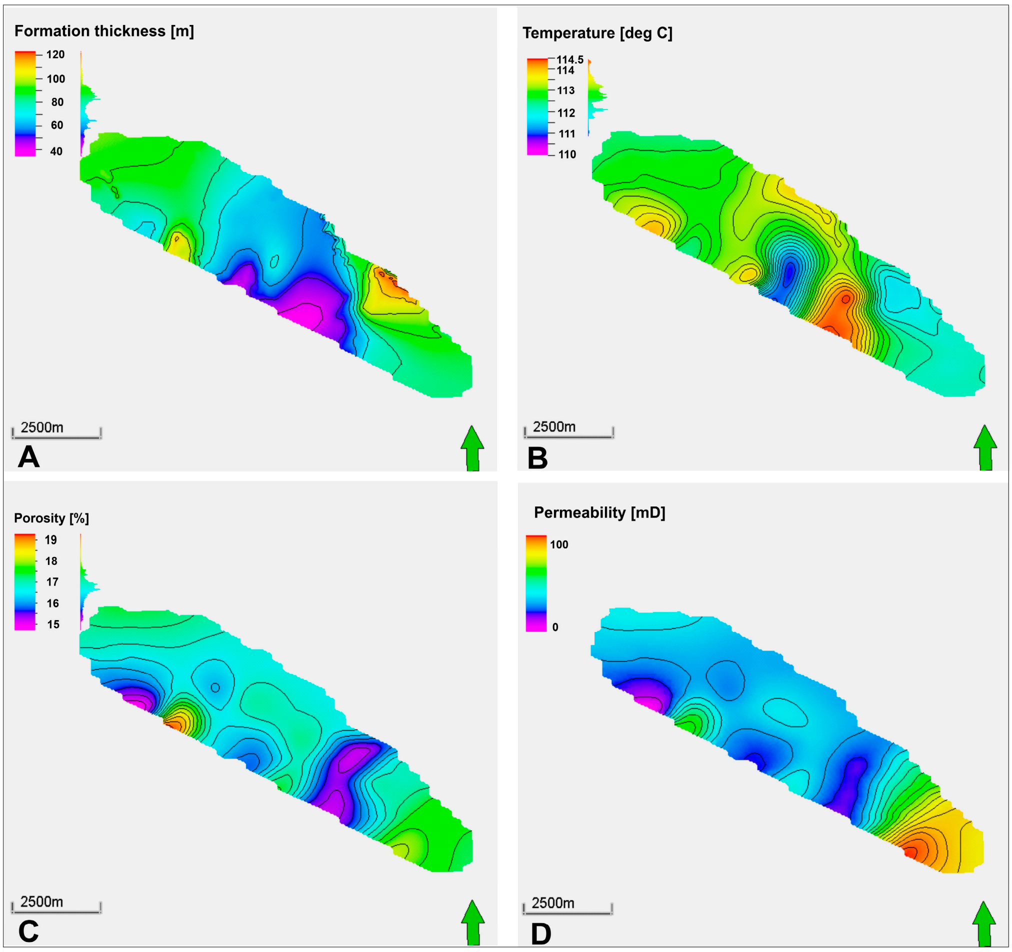

Figure 2. Visualization maps of thickness (**A**), average temperature (**B**), average porosity (**C**), and permeability (**D**) in the sandstone gas reservoir.

3.1.5. Recoverable Heat

Once the HIP was calculated, a recoverable heat (Hrec) was estimated with the use of the equation [42]:

$$\mathrm{Hrec} = \frac{(\mathrm{HIP} \times \mathrm{C_e} \times \mathrm{R_g})}{(\mathrm{T_{live}} \times \mathrm{P_f})} \tag{2}$$

where:
C_e—conversion efficiency factor (in parts per unit),
R_g—a recovery factor being a ratio of recoverable energy with the current technological a techno-economic condition to the total resource available in the reservoir (in parts per unit),
T_{live} and P_f—project lifetime (in seconds) and plant factor (in parts per unit), respectively.

The recovery factor was calculated using the formula proposed by Franco and Donatini [43]:

$$\mathrm{R_g} = \frac{(\mathrm{V} \times (0.5 \times \varphi \times 1) \times \rho_\mathrm{F}) \times (\Delta\mathrm{HR} - \Delta\mathrm{HS})}{\mathrm{HIP}} \tag{3}$$

where:
V—stands for the rock volume (m^3),
φ—the effective porosity (parts per unit),
ρ_F —working fluid density (kg/m^3),
$\Delta HR - \Delta HS$, effective enthalpy after heat extraction to the surface.

The recoverable heat was calculated for the geothermal system's lifetime of 50 years based on the spatial distribution of petrophysical parameters (i.e., effective porosity and permeability) and rock volumetric parameters (i.e., rock volume and rock formation temperature). Parameters such as enthalpy and rock-fluid system properties were determined based on the literature.

The density of the rock matrix and reservoir fluids was determined based on the results of the density measurements of the brines and core material (unpublished well reports). The density of working fluids was assumed, neglecting the operational conditions, injection, and production pressure, which are unknown at this stage of the work. The heat capacities of both rocks and fluids were based on the literature research [44] and specified for particular reservoir lithology (Table 1) [45,46].

Table 1. Assumed in the model values of rock, brine, and supercritical CO_2 heat capacity, rock and brine densities.

Reservoir	Specific Heat Capacity of Rock (kJ/kg°C)	Specific Heat Capacity of Brine (kJ/kg°C)	Specific Heat Capacity of Supercritical CO_2 (kJ/kg°C)	Density of Rock Matrix (kg/m^3)	Density of Brine (kg/m^3)
Sandstone reservoir	0.82	3.22	2.05	2650	1230
Carbonate reservoir	0.96	3.75	2.05	2710	1070

The temperature at the reservoir top, Tr, was determined based on the rock formation temperature well-logs. At the same time, T0 was selected as the ground surface temperature (GST) (Table 2) [25].

The enthalpy was determined by taking the investigated reservoir rocks' average initial pressure, temperature conditions, surface conditions, and fluid system assumptions based on the literature [47,48]. The obtained results are listed in Table 2.

Table 2. Assumed enthalpy for supercritical CO_2 determined for the temperature and pressure conditions in the analyzed reservoir formations.

Reservoir/Field	Average Reservoir Temperature (°C)	Average Annual Temperature at the surface (°C)	Average Reservoir Pressure (bar)	Enthalpy for the Reservoir Conditions for CO_2 System (kJ/kg)	Enthalpy at the Surface for CO_2 System (kJ/kg)
Sandstone reservoir	110	9.4	340	−100	−305
Carbonate reservoir	105	8	310	−120	−320

3.2. Classification of Potential Geothermal Plays with Generalized c-Means (GFCM)

The classification of potential geothermal plays was performed with the generalized c-means (GFCM) method, an extension of Fuzzy c-means (FCM) [49]. This unsupervised technique classifies observations by grouping similar data points into clusters in a predefined feature space. Clustering is achieved using an algorithm that iteratively minimizes total intra-cluster variations based on a cost function that depends on the Euclidean distance between the data point and the cluster center [50]. Unlike hard clustering methods, where one observation belongs to only one cluster (e.g., k-means), the FCM method allows the observation to have a relationship with many groups with a high membership probability, making the technique more reasonable in real-world applications [51]. In a final fuzzy membership matrix, assigning a cluster is determined based on the maximum coefficient of the data point over all clusters. The improvement of GFCM over FCM lies in an extra beta parameter that boosts the algorithm to accelerate convergence and allows for less fuzzy results. The beta parameter controls the effectiveness of the membership degree function, adjusting the fuzzy membership matrix at each iteration [52]. Such an approach is often used to overcome the uncertainty of noisy data by identifying outliers in feature space [49].

The GFCM clustering was conducted on three parameters: porosity, permeability, and computed recoverable heat for 50 years for a water system (Equation (2)). The parameters were averaged and mapped for the reservoir interval. The first two parameters define storage and filtration potential as crucial for the utilization of geothermal resources. The third one integrates many geothermal features that help understand potential locked-in geothermal plays.

Before clustering, the dataset for carbonate and sandstone reservoirs was scaled and centered. This operation makes the selected variables comparable. The beta parameter was derived by testing the possible values between 0 and 1 with a step of 0.05. The value of beta was chosen to minimize the Xie–Beni index—the parameter often used for evaluating the quality of FCM cluster partitioning. This parameter validates fuzzy partitions by taking into account the geometrical features of clusters, such as their compactness and separateness, which are measured using intra-cluster deviations and inter-cluster distance [53]. The obtained beta values for the datasets representing carbonate and sandstone reservoirs equal 0.54 and 0.57, respectively. The number of clusters was arbitrarily set to represent six potential geothermal plays.

4. Results and Discussion

This study investigated two different rock formations from two locations: the depleted gas reservoir from the Rotliegend sandstone formation and the depleted oil field in the carbonate reservoir. The relation between porosity and permeability parameters places both analyzed rock formations within the enhanced geothermal systems group [4] with distinction into a reservoir with strong dual porosity in the case of a fracture carbonate reservoir and a classic porous sandstone reservoir (Figure 3).

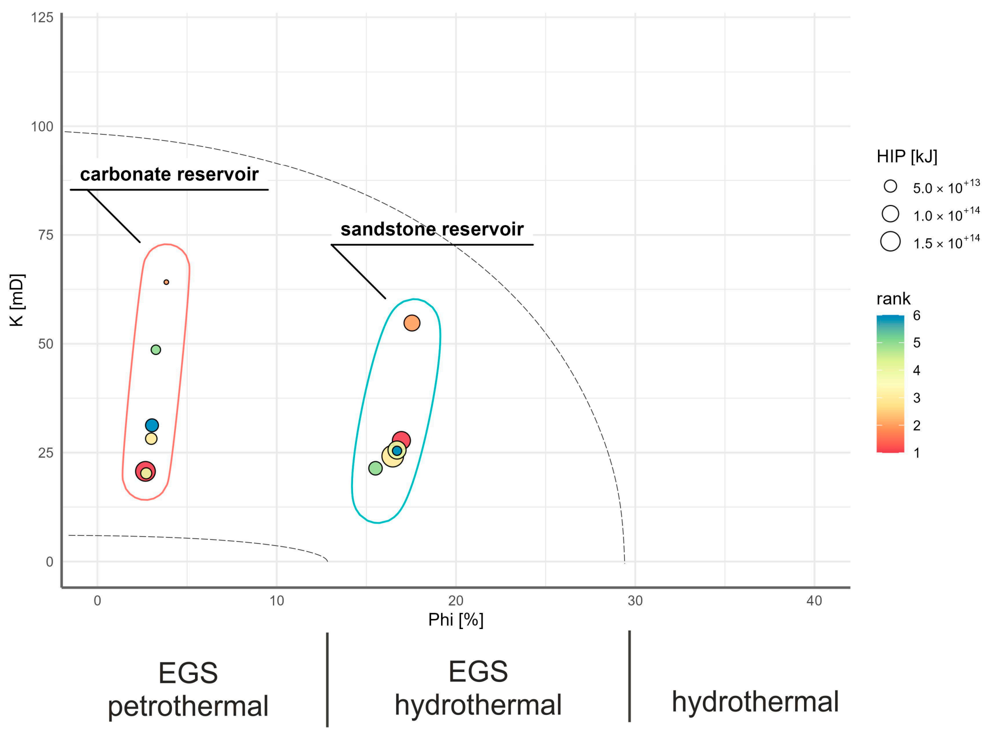

Figure 3. Porosity–Permeability relation for geothermal plays with marked HIP and rank results from GFCM clustering.

The geothermal potential of both reservoir rocks was investigated under the assumption of two working heat-transmission fluids—water and CO_2—in a supercritical state. The GFCM clustering results for both fields were arranged using Hrec (water system) and ranked from the most prospective (1) to the least promising (6). Previously, clustering methods were used to select hidden signatures representative of the geothermal resource and delineate geothermal/non-geothermal sites [31,32,36].

The carbonate reservoir is highly heterogeneous with a complex tectonic setting that divides the studied area into three separate blocks (I–III), of which only two seem to be prospective from a geothermal point of view (Figure 4).

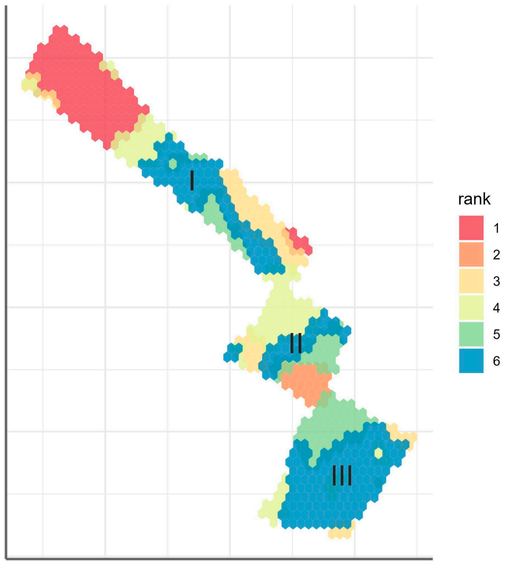

Figure 4. Potential geothermal plays from GFCM clustering for carbonate reservoir.

The area with the highest Hrec (rank 1) is located primarily on the edges of the elongated block (marked as I). Although the median Hrec in voxel for the zone ranked 1 is the highest among the clusters (~0.31 kW for water and ~0.07 kW for CO_2), these areas suffer from low porosity and moderate permeability of fracture type (median 2.7% and 21 mD) (Figure 5, Table 3). Such features may require EGS technology like hydraulic fracturing to improve fluid circulation and heat transfer to the surface. Another drawback of the elongated block is the lack of existing infrastructure, with only one well in the central part of the block (Figure 6). Drilling an extra well to create a geothermal doublet would significantly increase the investment cost of a potential geothermal plant. These issues eliminate block I as the primary target for heat production.

Table 3. Median voxel values for the key reservoir parameters for designated GFCM classes.

GFCM Rank	Median K (mD)	Median Phi (%)	Median HIP (TJ)	Median Hrec50 Water (kW)	Median Hrec50 CO_2 (kW)	Median Temp. (°C)
1	20.7	2.7	2.45	0.313	0.074	108
2	64.1	3.8	1.08	0.197	0.046	108
3	28.2	3.0	1.35	0.192	0.047	108
4	20.2	2.7	0.80	0.103	0.024	107
5	48.6	3.3	0.57	0.089	0.022	107
6	31.3	3.0	0.50	0.073	0.017	107

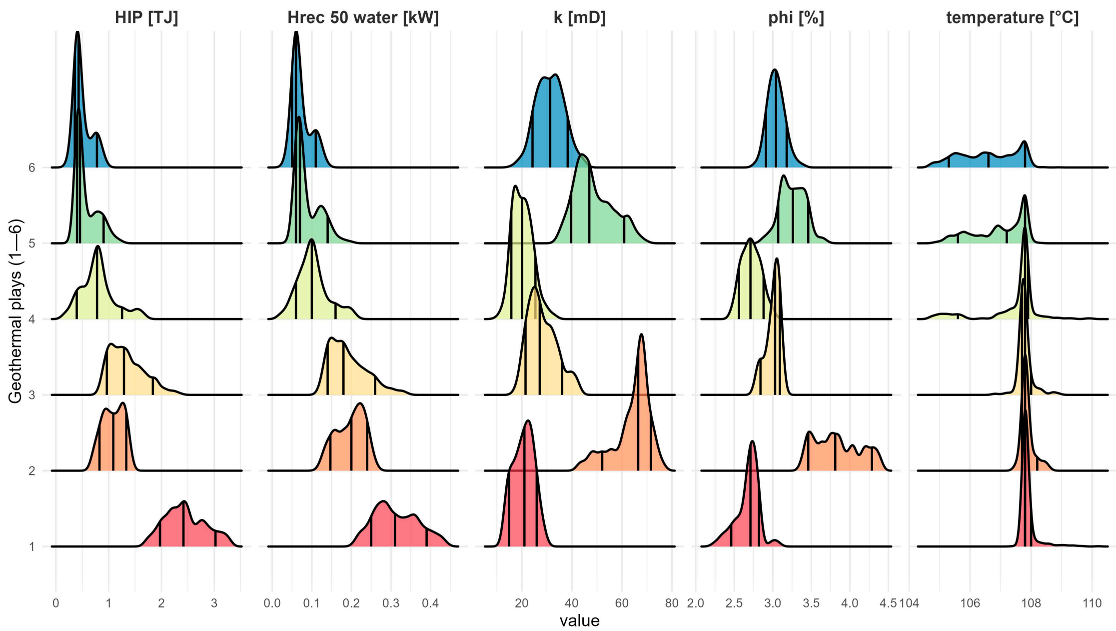

Figure 5. Density plots with key reservoir parameters and marked p10, p50, and p90 for carbonate reservoir. Colors define GFCM geothermal plays.

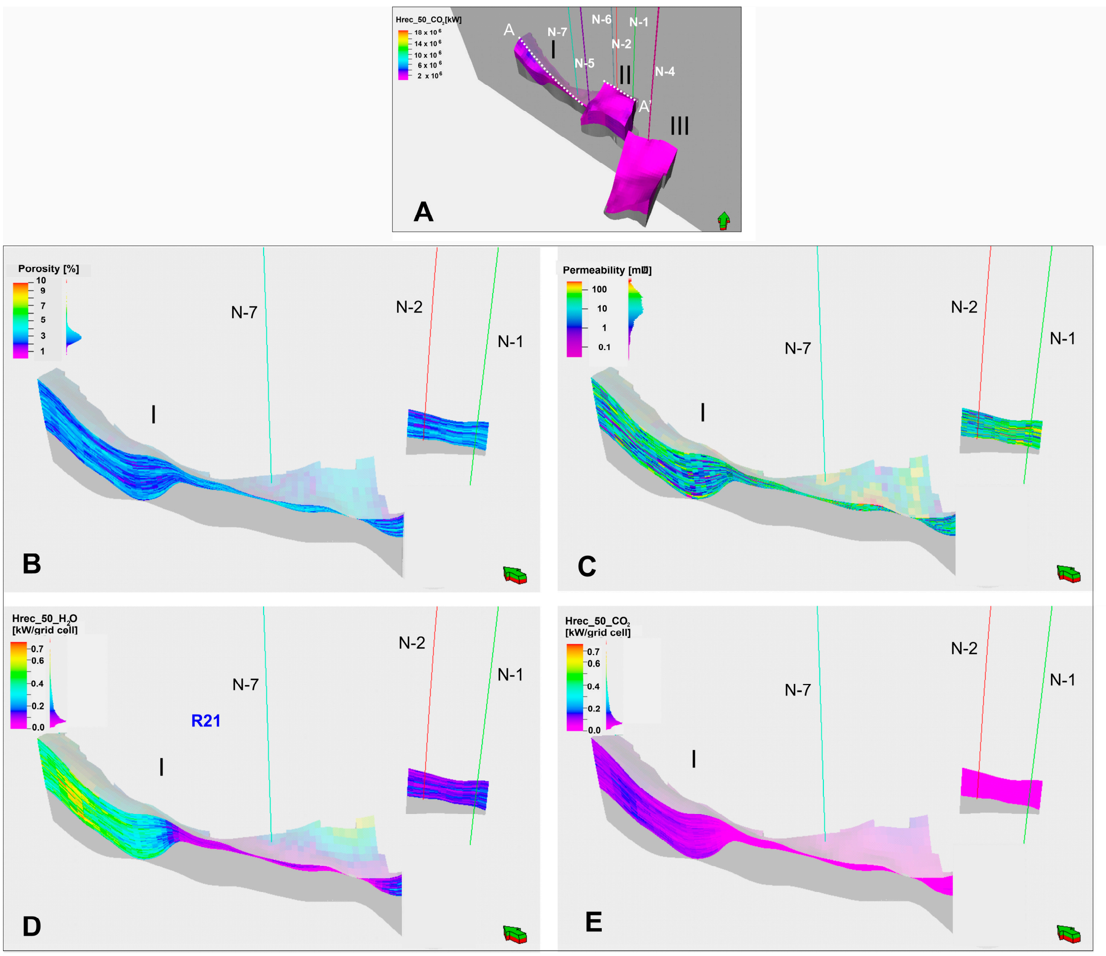

Figure 6. Visualization of the 3D distribution at cross-section A-A′ (**A**) of the reservoir porosity (**B**), permeability (**C**), and recoverable heat estimated for 50 years of a lifetime for water (**D**), and CO_2 working fluid (**E**) in the analyzed geothermal system in carbonate system formation.

The heat production from the middle square block (marked as II) seems to be more promising. The block creates a mixture of almost all clusters with a significant phi, k, and Hrec variety. The most promising zone of this block is located in its Southern part (Figure 7). The areas marked with 2 still have high voxel Hrec (median ~0.2 kW for water and ~0.05 kW for CO_2) but have higher porosity and permeability (median 3.8%, 64 mD) compared to areas ranked with 1 (Figure 5, Table 3). Block II was drilled by three wells with well-documented oil production histories (unpublished well reports) and hydraulic communication between them. This feature, together with a good thickness (median 201.82 m) and high temperature, makes the described isolated block a potential candidate for heat production with a triplet well system in the studied carbonate field (Figure 7). To maximize heat production, the injection well should be picked based on the highest HIP and Hrec (wells N1 and N5).

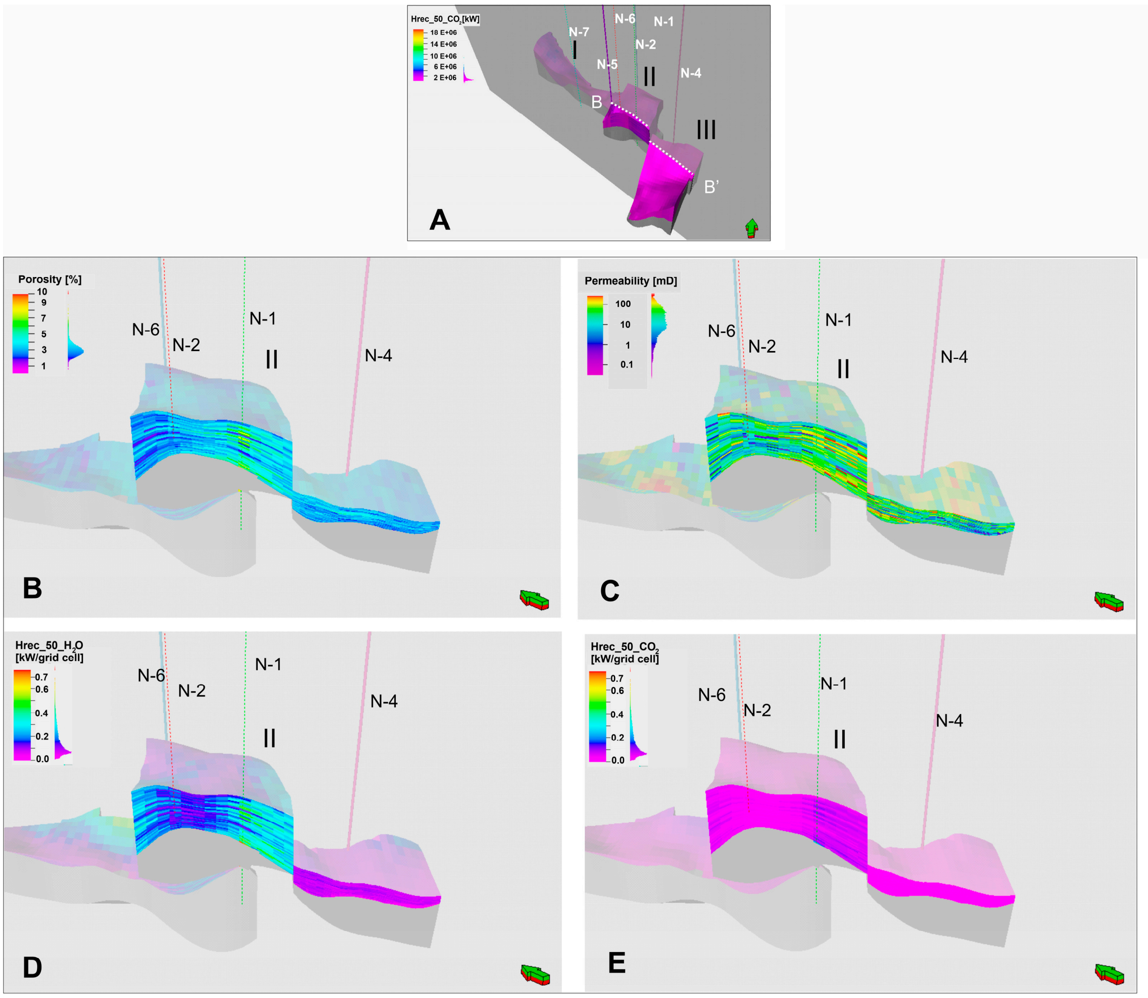

Figure 7. Visualization of the 3D distribution at cross-section B-B′ (**A**) of the reservoir porosity (**B**), permeability (**C**), and recoverable heat estimated for 50 years of a lifetime for water (**D**) and CO_2 working fluid (**E**) in the analyzed geothermal system in carbonate system formation.

Block III was excluded from the investigation due to the predominance of areas with ranks 5 and 6 with the lowest Hrec (~two times lower than rank 2) and a lack of existing infrastructure (Figures 5 and 8).

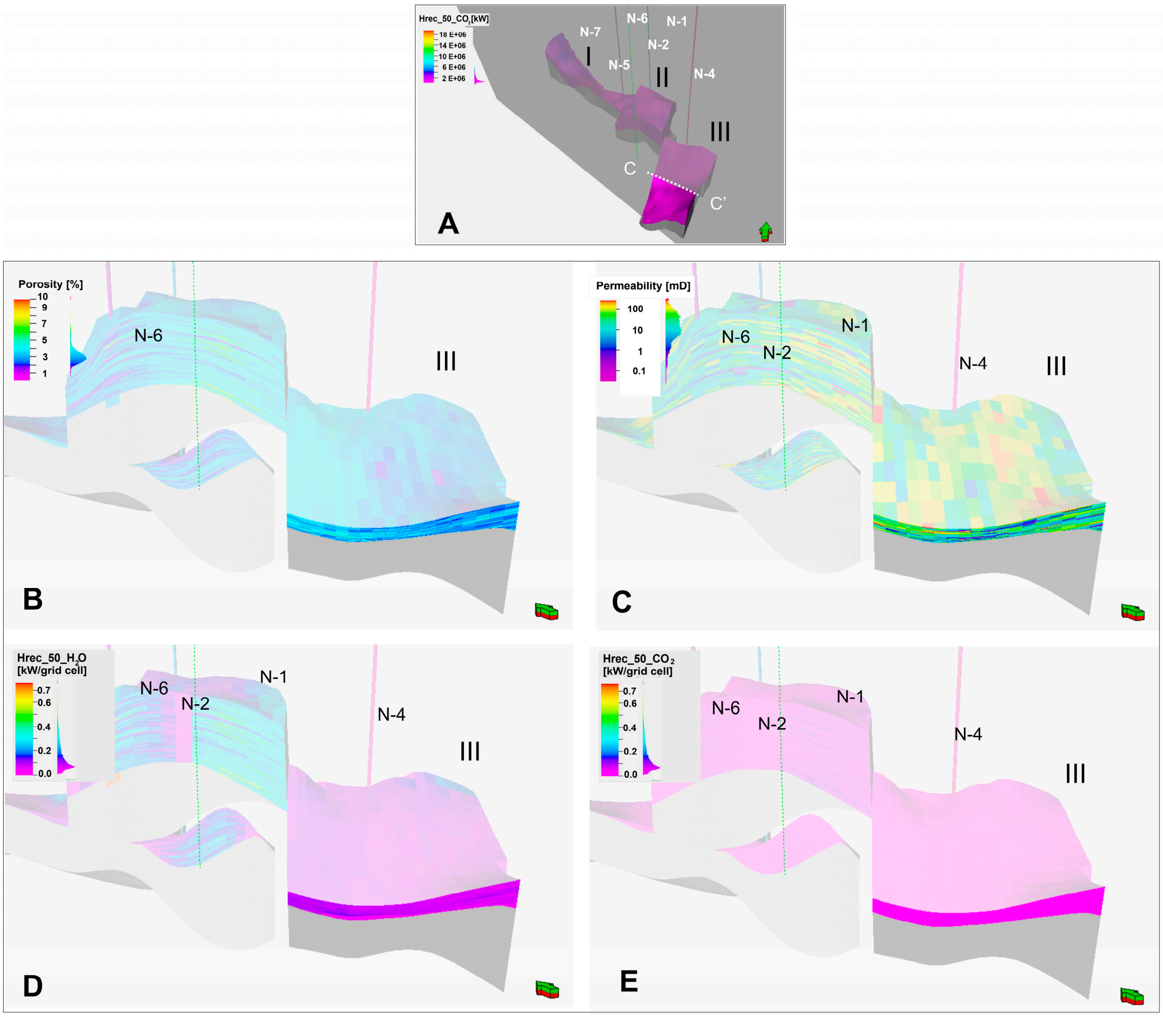

Figure 8. Visualization of the 3D distribution at cross-section C-C′ (**A**) of the reservoir porosity (**B**), permeability (**C**), and recoverable heat estimated for 50 years of lifetime for water (**D**) and CO_2 working fluid (**E**) in the analyzed geothermal system in carbonate system formation.

The conventional sandstone reservoir from the Foresudetic Monocline is much more homogeneous than the carbonate one. The spread of porosity across the clusters 1–6, varies from 15.5 to 17% (Figures 9 and 10, Table 4). The low variance is also observed in the case of permeability, which ranges from 21.4 to 54.8 mD (Figure 10). However, the geothermal potential expressed in Hrec varies across the field's longitudinal axis, and the difference is almost doubled between rank 1 and rank 6 areas (Figures 9 and 10). This feature is directly linked to the formation thickness and slightly greater depth and temperature of the zones with higher Hrec (Figure 11).

Table 4. Median voxel values for the key reservoir parameters for designated GFCM classes.

GFCM Rank	Median K (mD)	Median Phi (%)	Median HIP (TJ)	Median Hrec50 Water (kW)	Median Hrec50 CO_2 (kW)	Median Temp. (°C)
1	27.8	17.0	11.0	10.4	1.86	113
2	54.8	17.5	9.89	10.0	1.08	112
3	24.2	16.5	10.7	9.61	1.92	113
4	25.6	16.7	8.16	7.85	1.77	113
5	21.4	15.5	7.63	6.87	1.51	114
6	25.4	16.7	5.78	5.46	1.50	113

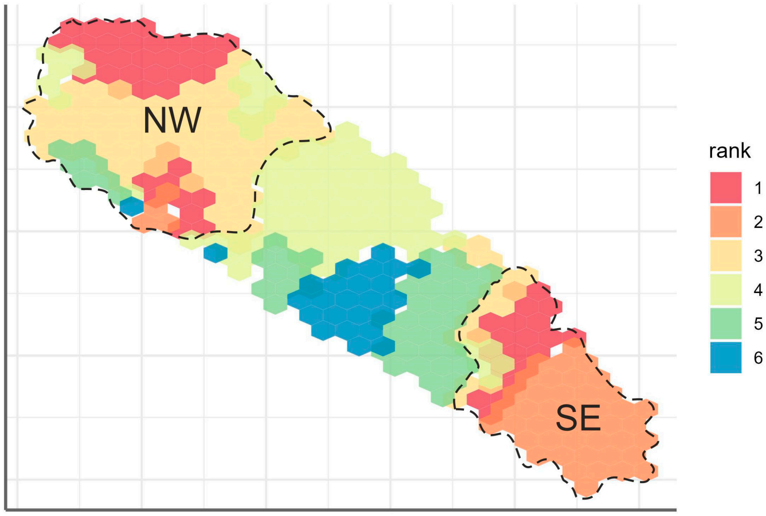

Figure 9. Potential geothermal plays from GFCM clustering for sandstone reservoir.

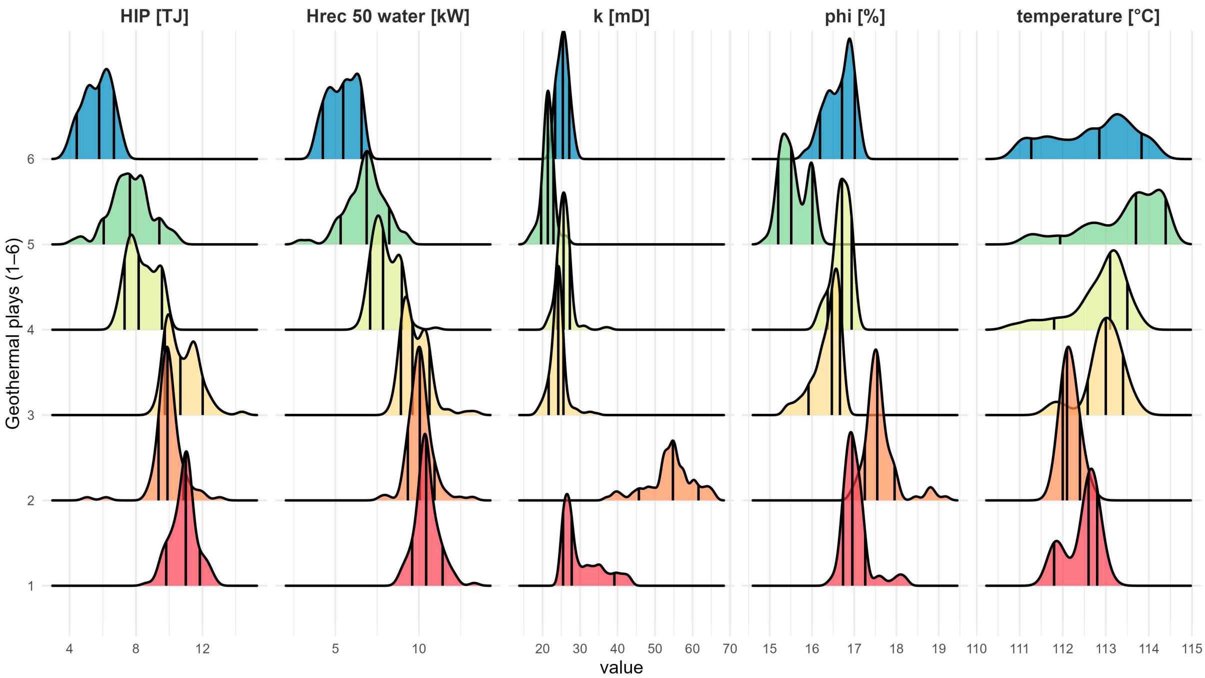

Figure 10. Density plots with key reservoir parameters and marked p10, p50, and p90 for sandstone reservoir. Colors define GFCM geothermal plays.

The median Hrec in voxel for areas marked with 1–3 (Figure 9) has comparable values ranging from ~10.4 to ~9.61 kW for water (for CO_2 ~1.92–1.08 kW). These areas occur at the edges of the field and are separated by a central part where zones ranked 4–6 dominate (Figure 9). Areas marked with rank 4–6 have significantly lower Hrec ranging from ~7.85 to ~5.46 kW for water (for CO_2 ~1.77–1.50 kW) (Figure 10, Table 4).

The entire field is covered with a substantial number of wells, with well-documented gas production histories (unpublished well reports) that provide suitable facilities for potential geothermal doublets or more complex systems [54]. A decreased Hrec zone in the central area of the field may suggest that the most effective heat production would be achieved through two separate geothermal systems with doublets located at the NW and SE edges of the field, within the boundary of zones marked with rank 1–3 (Figure 9).

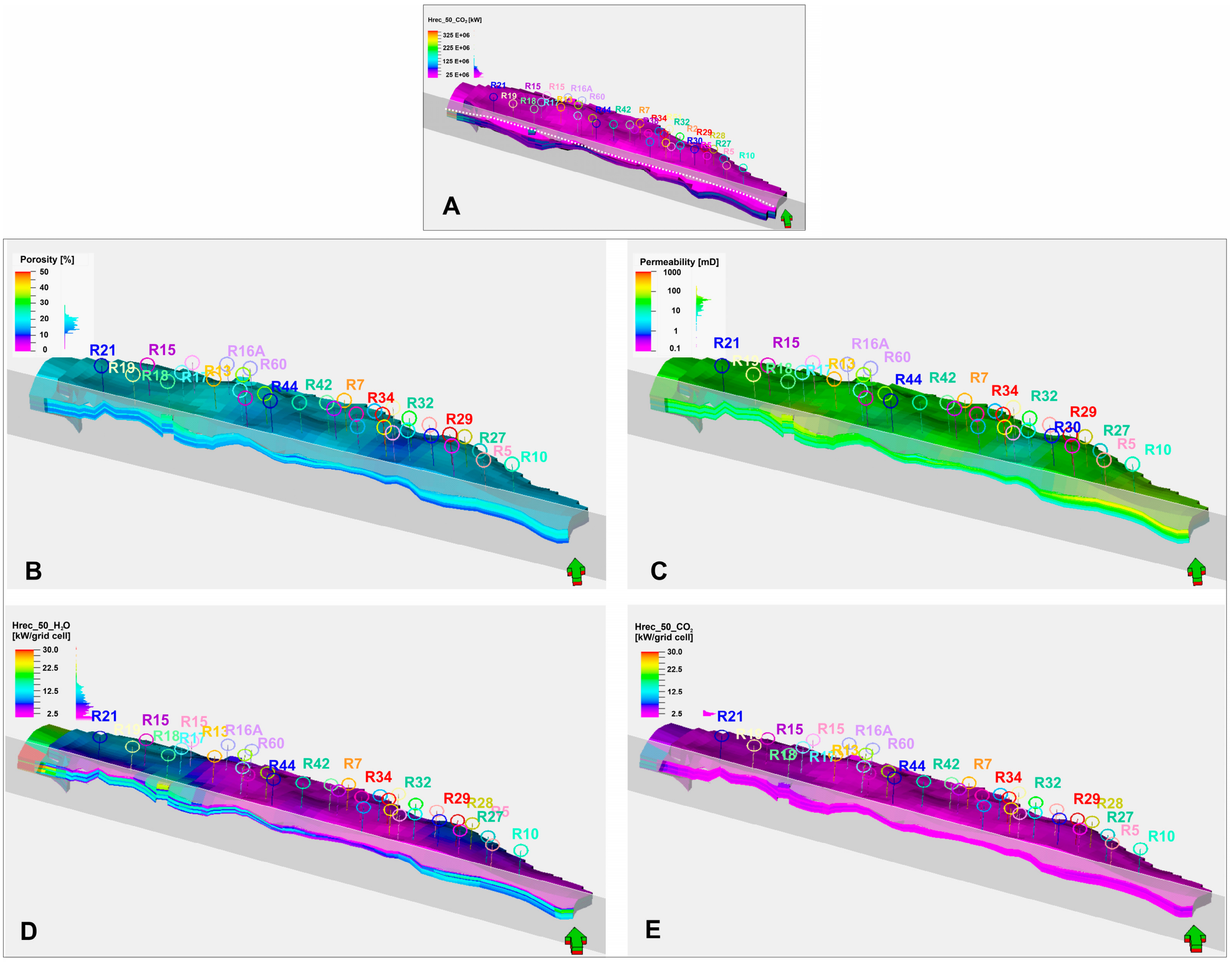

Figure 11. Visualization of the 3D distribution at cross-section (**A**) of the reservoir porosity (**B**), permeability (**C**), and recoverable heat estimated for 50 years of geothermal system lifetime Hrec estimated for the H_2O (**D**) and CO_2 € as a working fluid (**E**) in the analyzed geothermal system in Rotliegend sandstone formation.

The characteristics of selected regions with the highest geothermal potential is presented in Table 5.

Table 5. Characteristics of the total geothermal resources for selected regions with the highest geothermal potential.

	K (mD)	Phi (%)	Temp. (°C)	HIP H_2O (PJ)	HIP CO_2 (PJ)	Hrec 50 year H_2O (MW)	Hrec 50 year CO_2 (MW)
Sandstone reservoir—NW							
Min	4.3	11.10	102.4	207.79	155.68	14.85	2.76
Max	86.8	27.06	117.9	245.48	191.43	36.08	6.95
Mean	27.98	17.37	111.9	227.85	176.54	23.16	4.36
Sandstone reservoir—SE							
Min	0.04	102.1	726	170.73	135.53	23.00	4.04
Max	195.00	23.20	117.8	208.71	168.33	26.83	4.82
Mean	47.00	17.10	111.9	197.34	153.55	19.76	3.51
Carbonate reservoir—central block (II)							
Min	0.03	0.60	104.3	73.35	72.38	0.22	0.05
Max	355.00	8.20	111.0	81.24	77.66	3.01	0.70
Mean	37.00	3.10	107.8	76.76	75.15	1.12	0.26

Although both fields considered belong to EGS, the recoverable heat for the studied sandstone reservoir is approximately three orders higher than the carbonate field (Figure 3). This difference results from three aspects that distinguish these two fields. The most evident first is the available volume of rock with the best Hrec potential (rank 1–3). The second one can be related to the higher temperature of the sandstone field production zones (~110 °C vs. ~105 °C for the carbonate field). Finally, a significant difference in storage potential (~17% in sandstone vs. ~3% in a carbonate reservoir) is essential for geothermal resources estimation.

The sandstone field is much more prospective for successful geothermal system development. The potential Hrec for water for NW and SE regions equals 23.16 and 19.76 MW for 50 years lifetime (Table 5). For CO_2, this value is about four times lower and gives 4.36 and 3.51MW from NW and SE regions, respectively (Table 5). The number of existing wells in a field provides many options for an effective doublet configuration.

The central block of the carbonate field can potentially provide approximately 1.12 MW for 50 years for the conventional water system and about 0.26 MW for CO_2 (Table 5). Because the block has only three wells and a restricted area constrained by a fault system, the configuration of the injection-production doublet/triplet is highly limited.

Although Hrec for CO_2 is about four times lower than for water, CO_2 seems to be a promising working fluid regarding the EOR and/or potential CCS that could be coupled with geothermal energy acquisition [14,55]. The hydro-thermal reservoir scale numerical simulation for the Soultz–sous–Forets revealed that, compared to the water, CO_2 shows lower temperature reduction in the faulted and leakage zones for 50 years of operation, making CO_2 a more suitable working fluid in this particular case [18]. However, a big concern with the injection of CO_2 is its negative effect on well construction, which leads to alloy and cement corrosion [56–58]. The interactions between the injected CO_2 and the formation water can induce salt precipitation, which can potentially cause reservoir damage and subsequently affect the flow behavior [59].

The above study estimates the geothermal potential in two distinct reservoirs with varying geological settings, temperatures, and pressure conditions. This estimation was performed using static geological and parametric models and machine learning tools. However, to gain a deeper understanding of the heat extraction mechanism and effectively compare water and CO_2 geothermal systems, it is important to consider the near wellbore effects, which have been identified as having a significant impact on energy acquisition [18,60–62]. To achieve this, further research plans to conduct a more comprehensive analysis incorporating numerical modeling, specifically hydro-thermal-mechanical simulations, on a reservoir scale. This approach will provide a more detailed and accurate assessment of the geothermal system's performance and response.

5. Conclusions

Both analyzed reservoir formations—the Rotliegend sandstone formation and the Visean carbonate complex—fall into the EGS group.

The GFCM clustering based on porosity, permeability, and Hrec for water system produced groups of different geothermal reservoir characteristics. Among the three analyzed blocks of the carbonate reservoir, the central one is the most promising. Block II has Hrec of approximately 1.12 and 0.26 MW during 50 years of geosystem lifetime for H_2O and CO_2 as working fluids, respectively, but also existing infrastructure in the area. However, the transport properties in block II are weak and would require EGS technology to improve fluid circulation and heat transfer to the surface.

In the Rotliegend sandstone reservoir, two prospective zones were determined. They are located in the NW and SE regions of the investigated area. For both regions, the estimated Hrec was determined to be approximately 23.16 MW and 4.36 MW (NW region) and 19.76 MW and 3.51 MW (SE region), using H_2O and CO_2 as working fluids, respectively, during 50 years of the systems' lifetime. As there is already a dense well network, the abundance of the wells in this case was not considered as important during optimal zone location for geothermal well system placement. Both regions have high porosity and permeability, which provide good storage and transport properties for the working fluid.

Among the analyzed H_2O and CO_2 as heat transfer working fluids, H_2O has more potential for heat recovery. Applying H_2O as a working fluid has the ability to provide over four times more heat than CO_2 for the studied Visean carbonate reservoir and over five times more heat in the case of the Rotliegend sandstone reservoir.

Although identified as EGS due to their different lithology and petrophysical characteristics, the investigated rock formations exhibit different geothermal potential, with the superior advantage of Rotliegend sandstones. This advantage results from reservoir temperature, storage potential, transfer properties, and an existing well network that can be easily adjusted for geothermal heat production.

The obtained results and future simulation studies can reduce the uncertainty and costs associated with geothermal energy development.

Author Contributions: Conceptualization, T.T. and M.S.-V.; methodology, T.T. and M.S.-V.; software, T.T. and M.S-V.; validation, T.T. and M.S.-V.; formal analysis, T.T. and M.S.-V.; investigation, T.T. and M.S.-V.; resources, R.K.; data curation, T.T. and M.S.-V.; writing—original draft preparation, T.T., M.S.-V. and R.K.; writing—review and editing, T.T., M.S.-V. and R.K.; visualization, T.T. and M.S.-V.; supervision, T.T., M.S.-V. and R.K.; project administration, T.T. All authors have read and agreed to the published version of the manuscript.

Funding: The study was financed based on the statutory work entitled: Analiza możliwości pozyskania energii geotermalnej ze złóż naftowych—the work of the Oil and Gas Institute-National Research Institute (OGI-NRI) commissioned by the Ministry of Education and Science; order number: 0052/SG/2022.

Data Availability Statement: Third Party Data. Restrictions apply to the availability of these data. Data were obtained from PKN ORLEN PGNiG Exploration and Production Division and are available from the authors with the permission of PKN ORLEN PGNiG Exploration and Production Division.

Acknowledgments: The authors thank PKN ORLEN PGNiG Exploration and Production Division for indicating the areas of investigation and all necessary data for modeling. The authors are also grateful to Piotr Łętkowski from the OGI-NRI for helping to adapt the Rotliegend sandstone reservoir to be compatible with Petrel software, and to Krzysztof Sowiżdżał, and Marek Stadtmüller, from the OGI-NRI for providing petrophysical models from the carbonate field.

Conflicts of Interest: The authors declare no conflict of interest.

References

1. European Commission A Policy Framework for Climate and Energy in the Period from 2020 to 2030. Available online: https://data.consilium.europa.eu/doc/document/ST56442014REV1/EN/pdf (accessed on 19 May 2023).
2. Barbier, E. Geothermal Energy Technology and Current Status: An Overview. *Renew. Sustain. Energy Rev.* **2002**, *6*, 3–65. [CrossRef]
3. Le Brun, M.; Hamm, V.; Lopez, S.; Ungemach, P.; Antics, M.; Ausseur, J.Y.; Cordier, E.; Giuglaris, E.; Goblet, P.; Lalos, P. Hydraulic and Thermal Impact Modelling at the Scale of the Geothermal Heating Doublet in the Paris Basin, France. In Proceedings of the Thirty-Sixth Workshop on Geothermal Reservoir Engineering, Stanford, CA, USA, 31 January–2 February 2011; pp. 1–12.
4. Moeck, I.S. Catalog of Geothermal Play Types Based on Geologic Controls. *Renew. Sustain. Energy Rev.* **2014**, *37*, 867–882. [CrossRef]
5. Limberger, J.; Boxem, T.; Pluymaekers, M.; Bruhn, D.; Manzella, A.; Calcagno, P.; Beekman, F.; Cloetingh, S.; van Wees, J.D. Geothermal Energy in Deep Aquifers: A Global Assessment of the Resource Base for Direct Heat Utilization. *Renew. Sustain. Energy Rev.* **2018**, *82*, 961–975. [CrossRef]
6. Archer, R. Geothermal Energy. In *Future Energy*; Elsevier: Amsterdam, The Netherlands, 2020; pp. 431–445.
7. Zarrouk, S.J.; McLean, K. *Geothermal Well Test Analysis: Fundamentals, Applications and Advanced Techniques*; Zarrouk, S.J., McLean, K., Eds.; Academic Press: New York, NY, USA, 2019; ISBN 9780128149478.
8. Aydin, H.; Merey, S. Potential of Geothermal Energy Production from Depleted Gas Fields: A Case Study of Dodan Field, Turkey. *Renew. Energy* **2021**, *164*, 1076–1088. [CrossRef]
9. Daniilidis, A.; Nick, H.M.; Bruhn, D.F. Interdependencies between Physical, Design and Operational Parameters for Direct Use Geothermal Heat in Faulted Hydrothermal Reservoirs. *Geothermics* **2020**, *86*, 101806. [CrossRef]
10. Daniilidis, A.; Nick, H.M.; Bruhn, D.F. Interference between Geothermal Doublets across a Fault under Subsurface Uncertainty; Implications for Field Development and Regulation. *Geothermics* **2021**, *91*, 102041. [CrossRef]

11. Daniilidis, A.; Alpsoy, B.; Herber, R. Impact of Technical and Economic Uncertainties on the Economic Performance of a Deep Geothermal Heat System. *Renew. Energy* **2017**, *114*, 805–816. [CrossRef]
12. Pruess, K. Enhanced Geothermal Systems (EGS) Using CO_2 as Working Fluid-A Novel Approach for Generating Renewable Energy with Simultaneous Sequestration of Carbon. *Geothermics* **2006**, *35*, 351–367. [CrossRef]
13. Miranda-Barbosa, E.; Sigfússon, B.; Carlsson, J.; Tzimas, E. Advantages from Combining CCS with Geothermal Energy. *Energy Procedia* **2017**, *114*, 6666–6676. [CrossRef]
14. Wu, Y.; Li, P. The Potential of Coupled Carbon Storage and Geothermal Extraction in a CO_2-Enhanced Geothermal System: A Review. *Geotherm. Energy* **2020**, *8*, 19. [CrossRef]
15. Li, M.X.; Ricard, L.P.; Underschultz, J.; Freifeld, B.M. Reducing Operational Costs of CO_2 Sequestration through Geothermal Energy Integration. *Int. J. Greenh. Gas Control* **2016**, *44*, 238–248. [CrossRef]
16. Cui, G.; Ren, S.; Dou, B.; Ning, F. Geothermal Energy Exploitation from Depleted High-Temperature Gas Reservoirs by Recycling CO_2: The Superiority and Existing Problems. *Geosci. Front.* **2021**, *12*, 101078. [CrossRef]
17. The U.S. Department of Energy (DOE). Awards $8.4 Million for Accessing Geothermal Potential from Abandoned Oil and Gas Wells. Available online: https://www.energy.gov/eere/articles/doe-awards-84-million-accessing-geothermal-potential-abandoned-oil-and-gas-wells (accessed on 1 June 2023).
18. Singh, M.; Mahmoodpour, S.; Ershadnia, R.; Soltanian, M.R.; Sass, I. Comparative Study on Heat Extraction from Soultz-Sous-Forêts Geothermal Field Using Supercritical Carbon Dioxide and Water as the Working Fluid. *Energy* **2023**, *266*, 126388. [CrossRef]
19. Cheng, W.L.; Li, T.T.; Nian, Y.L.; Xie, K. Evaluation of Working Fluids for Geothermal Power Generation from Abandoned Oil Wells. *Appl. Energy* **2014**, *118*, 238–245. [CrossRef]
20. Donselaar, M.E.; Groenenberg, R.M.; Gilding, D.T. Reservoir Geology and Geothermal Potential of the Delft Sandstone Member in the West Netherlands Basin. In *Proceedings World Geothermal Congress*; International Geothermal Association: Bonn, Germany, 2015; pp. 19–25.
21. Sowiżdżał, A.; Górecki, W.; Hajto, M. Geological Conditions of Geothermal Resource Occurrences in Poland. *Geol. Q.* **2020**, *64*, 185–196. [CrossRef]
22. Różkowski, A. Gological Environmet of Geothermal Waters in the Productive Carboniferous Formation in the Upper Silesian Coal Basin (ASCB). In Proceedings of the Geothermal Energy in Underground Mines, Ustroń, Poland, 21–23 November 2001; pp. 51–62.
23. Sowizdzał, A.; Semyrka, R. Analyses of Permeability and Porosity of Sedimentary Rocks in Terms of Unconventional Geothermal Resource Explorations in Poland. *Geologos* **2016**, *22*, 149–163. [CrossRef]
24. Pajak, L.; Sowiżdżał, A.; Gładysz, P.; Tomaszewska, B.; Miecznik, M.; Andresen, T.; Frengstad, B.S.; Chmielowska, A. Multi-Criteria Studies and Assessment Supporting the Selection of Locations and Technologies Used in CO_2-Egs Systems. *Energies* **2021**, *14*, 7683. [CrossRef]
25. Górecki, W.; Szczepański, A.; Sadurski, A.; Hajto, M.; Papiernik, B.; Jan, S.; Sokołowski, A.; Strzetelski, W.; Haładus, A.; Kania, J.; et al. *Atlas of Geothermal Resources of Paleozoic Formations in the Polish, Lowlands*; Górecki, W., Ed.; AGH Akademia Górniczo-Hutnicza w Krakowie: Krakow, Poland, 2006; ISBN 978-83-88927-14-0.
26. Górecki, W.; Szczepański, A.; Sadurski, A.; Hajto, M.; Papiernik, B.; Jan, S.; Sokołowski, A.; Strzetelski, W.; Haładus, A.; Kania, J.; et al. *Geothermal Atlas of the Eastern Carpathians*; Górecki, W., Ed.; AGH University of Science and Technology in Krakow: Krakow, Poland, 2013; ISBN 978-83-88927-33-1.
27. Górecki, W.; Hajto, M.; Szczepański, A.; Sadurski, A.; Papiernik, B.; Jan, S.; Sokołowski, A.; Strzetelski, W.; Haładus, A.; Kania, J.; et al. *Atlas of Geothermal Waters and Energy Resources in the Western Carpathians*; Górecki, W., Ed.; AGH University of Science and Technology in Krakow: Krakow, Poland, 2011; ISBN 13 978-83-88927-21-8.
28. Górecki, W.; Hajto, M.; Papiernik, B.; Kuźniak, T.; Szczepański, A.; Sadurski, A.; Kozdra, T.; Soboń, J.; Jan, S.; Sokołowski, A.; et al. *Atlas of Geothermal Resources of Mesozoic Formations in the Polish Lowlands*; Górecki, W., Ed.; AGH University of Science and Technology in Krakow: Krakow, Poland, 2006; ISBN 978-83-88927-13-3.
29. Górecki, W.; Sowiżdżał, A.; Jasnos, J.; Papiernik, B.; Hajto, M.; Machowski, G.; Kępińska, B.; CZOPEK, B.; Kuźniak, T.; Kotyza, J.; et al. *Atlas Geotermalny Zapadliska Przedkarpackiego*; Górecki, W., Ed.; AGH Akademia Górniczo-Hutnicza w Krakowie: Kraków, Poland, 2012; ISBN 978-83-88927-27-0.
30. Okoroafor, E.R.; Smith, C.M.; Ochie, K.I.; Nwosu, C.J.; Gudmundsdottir, H.; Aljubran, M.J. Machine Learning in Subsurface Geothermal Energy: Two Decades in Review. *Geothermics* **2022**, *102*, 102401. [CrossRef]
31. Moraga, J.; Duzgun, H.S.; Cavur, M.; Soydan, H. The Geothermal Artificial Intelligence for Geothermal Exploration. *Renew. Energy* **2022**, *192*, 134–149. [CrossRef]
32. Yusuf, A.; San, L.H.; Abir, I.A. A Preliminary Geothermal Prospectivity Mapping Based on Integrated GIS, Remote-Sensing, and Geophysical Techniques around Northeastern Nigeria. *Sustainability* **2021**, *13*, 8525. [CrossRef]
33. Kiavarz, M.; Noorollahi, Y.; Samadzadegan, F.; Sharifi, M.A.; Itoi, R. Spatial Data Analysis for Exploration of Regional Scale Geothermal Resources. *J. Volcanol. Geotherm. Res.* **2013**, *266*, 69–83.
34. Mudunuru, M.K.; Ahmmed, B.; Rau, E.; Vesselinov, V.V.; Karra, S. Machine Learning for Geothermal Resource Exploration in the Tularosa Basin, New Mexico. *Energies* **2023**, *16*, 3098. [CrossRef]

35. Haklidir, F.; Haklidir, M. The Reservoir Temperature Prediction Using Hydrogeochemical Indicators By Machine Learning: Western Anatolia (Turkey) Case. In *Proceedings World Geothermal Congress*; International Geothermal Association: Bonn, Germany, 2021; pp. 1–5.
36. Vesselinov, V.V.; Ahmmed, B.; Mudunuru, M.K.; Pepin, J.D.; Burns, E.R.; Siler, D.L.; Karra, S.; Middleton, R.S. Discovering Hidden Geothermal Signatures Using Non-Negative Matrix Factorization with Customized k-Means Clustering. *Geothermics* **2022**, *106*, 102576. [CrossRef]
37. Levorsen, A.I. The Obscure and Subtle Trap. *Am. Assoc. Pet. Geol. Bull.* **1966**, *50*, 2058–2067.
38. Zawisza, L. Simplified Method of Absolute Permeability Estimation of Porous Beds. *Arch. Min. Sci.* **1993**, *38*, 343–352.
39. Herms, I.; Colomer, M.; Diepolder, G.W.; Piris, G.; Arnó, G.; Gómez-Rivas, E. 3D Modelling and Geothermal Potential Assessment of a Fractured Carbonate Reservoir in the South-Eastern Pyrenees. The Empordà Case Study in NE Catalonia—GeoERA HotLime Project. In *Proceedings World Geothermal Congress*; International Geothermal Association: Bonn, Germany, 2021; pp. 1–12.
40. Nathenson, M. Methodology of Determining the Uncertainty in the Accessible Geothermal Resource Base of Identified Hydrothermal Convection Systems. U.S. Geological Survey: Reston, VA, USA, 1978.
41. Muffler, P.; Cataldi, R. Methods for Regional Assessment of Geothermal Resources. *Geothermics* **1978**, *7*, 53–89. [CrossRef]
42. Piris, G.; Herms, I.; Griera, A.; Colomer, M.; Arnó, G.; Gomez-Rivas, E. 3DHIP-Calculator—A New Tool to Stochastically Assess Deep Geothermal Potential Using the Heat-In-Place Method from Voxel-Based 3D Geological Models. *Energies* **2021**, *14*, 7338. [CrossRef]
43. Franco, A.; Donatini, F. Methods for the Estimation of the Energy Stored in Geothermal Reservoirs. *J. Phys. Conf. Ser.* **2017**, *796*, 012025. [CrossRef]
44. Ramalingam, A.; Arumugam, S. Experimental Study on Specific Heat of Hot Brine for Salt Gradient Solar Pond Application. *Int. J. ChemTech Res.* **2012**, *4*, 956–961.
45. Robertson, E.C. *Thermal Properties of Rocks*; U.S. Geological Survey: Reston, VA, USA, 1988; pp. 88–441.
46. Hartlieb, P.; Toifl, M.; Kuchar, F.; Meisels, R.; Antretter, T. Thermo-Physical Properties of Selected Hard Rocks and Their Relation to Microwave-Assisted Comminution. *Miner. Eng.* **2016**, *91*, 34–41. [CrossRef]
47. Ishmael, M.P.E.; Lukawski, M.Z.; Tester, J.W. Isobaric Heat Capacity (Cp) Measurements of Supercritical Fluids Using Flow Calorimetry: Equipment Design and Experimental Validation with Carbon Dioxide, Methanol, and Carbon Dioxide-Methanol Mixtures. *J. Supercrit. Fluids* **2016**, *117*, 72–79. [CrossRef]
48. Allam, R.; Martin, S.; Forrest, B.; Fetvedt, J.; Lu, X.; Freed, D.; Brown, G.W.; Sasaki, T.; Itoh, M.; Manning, J. Demonstration of the Allam Cycle: An Update on the Development Status of a High Efficiency Supercritical Carbon Dioxide Power Process Employing Full Carbon Capture. *Energy Procedia* **2017**, *11*, 5948–5966. [CrossRef]
49. Karayiannis, N.B. Generalized Fuzzy C-Means Algorithms. In Proceedings of the IEEE 5th International Fuzzy Systems, New Orleans, LA, USA, 11 September 1996; pp. 1036–1042.
50. Zabihi, S.M.; Akbarzadeh-T, M.-R. Generalized Fuzzy C-Means Clustering with Improved Fuzzy Partitions and Shadowed Sets. *ISRN Artif. Intell.* **2012**, *2012*, 929085. [CrossRef]
51. Adhikari, S.K.; Sing, J.K.; Basu, D.K.; Nasipuri, M. Conditional Spatial Fuzzy C-Means Clustering Algorithm for Segmentation of MRI Images. *Appl. Soft Comput.* **2015**, *34*, 758–769. [CrossRef]
52. Ferraro, M.B.; Giordani, P.; Serafini, A. Fclust: An R Package for Fuzzy Clustering. *R J.* **2019**, *11*, 198–210. [CrossRef]
53. Muranishi, M.; Honda, K.; Notsu, A. Xie-Beni-Type Fuzzy Cluster Validation in Fuzzy Co-Clustering of Documents and Keywords. *Adv. Intell. Syst. Comput.* **2014**, *270*, 29–38.
54. Willems, C.J.L.; Nick, H.M. Towards Optimisation of Geothermal Heat Recovery: An Example from the West Netherlands Basin. *Appl. Energy* **2019**, *247*, 582–593. [CrossRef]
55. Freifeld, B.; Zakim, S.; Pan, L.; Cutright, B.; Sheu, M.; Doughty, C.; Held, T. Geothermal Energy Production Coupled with CCS: A Field Demonstration at the SECARB Cranfield Site, Cranfield, Mississippi, USA. *Energy Procedia* **2013**, *37*, 6595–6603. [CrossRef]
56. Ropital, F.; Kittel, J. Corrosion Evaluation of Steels Under Geothermal CO_2 Supercritical Conditions. In *Proceedings World Geothermal Congress*; International Geothermal Association: Bonn, Germany, 2021; pp. 1–4.
57. Milestone, N.B.; Bigley, C.H.; Durant, A.T.; Sharp, M.D.W. Effects of CO_2 on Geothermal Cements. *GRC Trans.* **2012**, *36*, 301–306.
58. Mundhenk, N.; Huttenloch, P.; Bäßler, R.; Kohl, T.; Steger, H.; Zorn, R. Electrochemical Study of the Corrosion of Different Alloys Exposed to Deaerated 80°C Geothermal Brines Containing CO_2. *Corros. Sci.* **2014**, *84*, 180–188. [CrossRef]
59. Cui, G.; Zhang, L.; Ren, B.; Enechukwu, C.; Liu, Y.; Ren, S. Geothermal Exploitation from Depleted High Temperature Gas Reservoirs via Recycling Supercritical CO_2: Heat Mining Rate and Salt Precipitation Effects. *Appl. Energy* **2016**, *183*, 837–852. [CrossRef]
60. Lei, H. Performance Comparison of H2O and CO_2 as the Working Fluid in Coupled Wellbore/Reservoir Systems for Geothermal Heat Extraction. *Front. Earth Sci.* **2022**, *10*, 819778. [CrossRef]

61. Zhong, C.; Xu, T.; Gherardi, F.; Yuan, Y. Comparison of CO_2 and Water as Working Fluids for an Enhanced Geothermal System in the Gonghe Basin, Northwest China. *Gondwana Res.* 2022, *in press*. [CrossRef]
62. Gudala, M.; Govindarajan, S.K.; Yan, B.; Sun, S. Comparison of Supercritical CO_2 with Water as Geofluid in Geothermal Reservoirs with Numerical Investigation Using Fully Coupled Thermo-Hydro-Geomechanical Model. *J. Energy Resour. Technol.* **2023**, *145*, 061302. [CrossRef]